WAVE-CURRENT INTERACTION IN FORMATION OF RIP CHANNEL SYSTEM

Y.Uchiyama[1], H. Kaida[1,] and D. Miyazaki[1]

ABSTRACT: Current effect on waves (CEW) is examined for formation of a rip channel system with a barotropic modeling framework based on Uchiyama *et al.* (2009). The model consists of an Eulerian phase-averaged shallow water equation with a vortex-force formalism, WKB ray equations for spectrum-peak waves, and a bed evolution equation with the Soulsby-Van Rijn's total sediment flux prescription. CEW acts on reducing the offshore extent of seaward rip currents through wave refraction on the currents, leading to modifying the budget of sediment flux and associated surf-zone topography. Inclusion of CEW results in shoaling rip channels, deepening offshore mounds, and elongating alongshore spacing of rip channels with normal incidence of offshore waves.

Keywords: Sediment transport, wave-current interaction, vortex-force formalism, barotropic numerical model.

INTRODUCTION

Rip channel system is a typical topographic feature of sandy beaches, occasionally being quite periodic in the alongshore direction, forming rhythmic patterns such as beach cusps emerged on the foreshore region. Rip currents and longshore currents are the pronounced driving forces that enhance self-organization of the rip channels through the interaction between wave-driven hydrodynamic modulation and associated morphological processes. Recent studies have agreed that current effect on waves (hereafter CEW) plays an essential role in changing rip currents (*e.g.*, Haas *et al*., 1999; Yu and Slinn, 2003, hereinafter YS03; Weir *et al.*, 2011) and longshore currents (*e.g.*, Özkan-Haller and Li, 2003; Uchiyama *et al*., 2009) through Doppler shift of wave frequency in dispersion relation and wave refraction (ray bending) by ambient currents. In particular, it has widely been accepted that CEW acts to attenuate the offshore extent of rip currents significantly. YS03 suggest that the work done by radiation stress in the wave energy balance equation is responsible for this reduction. Their result implies that reduced rip currents by CEW could modify resultant rip channel topography.

The present study is to analyze the evolution of rip channel system due to deformation of a longshore bar with a phase-averaged barotropic numerical model. Particular attention is paid to the influence of CEW. The model relies mainly on a novel mathematical framework by Uchiyama *et al*. (2009, 2010) based on the multi-scale asymptotic theory of the Eulerian wave-averaged vortex force formalism (McWilliams *et al*., 2004), accounting for the two-way mutual interaction between waves and currents around the surf zone. Differing from the traditional radiation stress formalism, it cleanly separates conservative (vortex force, wave set-down, Stokes-Coriolis force if necessary) and non-conservative (wave breaking, wave-enhanced bottom drag, boundary streaming, enhanced vertical and lateral mixing) wave effect on current (hereinafter WEC). An empirical total sediment load model proposed by Soulsby and Van Rijn (described in Soulsby, 1997) with a diffusive downslope transport effect is then utilized for evaluating sediment transport and associated morphological evolution (*e.g*., Garnier *et al.*, 2008).

This paper is organized into four sections. After the introduction, we present the mathematical framework of the coupled, barotropic wave-current-sediment model in Sec. 2. We then provide typical results and a brief discussion in Sec. 3 for the cases on a mobile sea floor where the strongest rip currents appear with normally incident offshore waves leading to rip channel systems with pronounced alongshore periodicity. Influences of CEW on the resultant beach topography are examined. We examine two cases of immobile beds to demonstrate CEW on the development of rip currents. Section 4 provides a summary of the present study.

METHODOLOGY

Phase-averaged Hydrodynamic Model

The hydrodynamic model is based on the one proposed in Uchiyama *et al*. (2009), consisting of the shallow-water equation for slowly-evolving Eulerian phase-averaged mass and momentum conservation:

$$\frac{\partial \zeta}{\partial t} + \nabla \cdot H\mathbf{u} = -\frac{\partial \hat{\zeta}}{\partial t} - \nabla \cdot \mathbf{U}^{\mathrm{st}} \tag{1}$$

[1] Department of Civil Engineering, Kobe University, 1-1 Rokkodai-Cho, Nada-ku, Kobe 657-8501, JAPAN

$$\frac{\partial \mathbf{u}}{\partial t}+\mathbf{u}\cdot\nabla\mathbf{u}+g\nabla\zeta=\mathbf{J}+\mathbf{B}-\mathbf{D} \tag{2}$$

where ζ is a phase-averaged, non-wave surface elevation, $\hat{\zeta}$ is the wave-induced, lowest-order Bernoulli pressure head representing the quasi-static sea-level response (*i.e.*, wave set down), $\mathbf{u} = (u, v)$ is a depth-averaged, Eulerian phase-averaged horizontal velocity, and g is the gravity. All the r.h.s. terms are wave forcing while those in the l.h.s. are the usual ones. The slowly varying sea surface elevation ζ^c and the total depth H are

$$\zeta^c=\zeta+\hat{\zeta} \tag{3}$$

$$H=h-z_b+\zeta^c \tag{4}$$

with the resting ocean depth, h, and a topographic perturbation, z_b, defined positive upward in case where the sea floor is mobile.

In Eq. (2) $\mathbf{J}$, $\mathbf{B}$ and $\mathbf{D}$ stand for the vortex-force term, breaker acceleration term (momentum transfer from wave to current due to depth-induced wave breaking) and the bottom drag term, respectively.

$$\mathbf{J}=-\hat{\mathbf{z}}\times\frac{1}{H}\mathbf{U}^{\mathrm{st}}\chi \tag{5}$$

$$\mathbf{B}=\frac{\varepsilon_b\mathbf{k}}{\rho H\sigma} \tag{6}$$

$$\mathbf{D}=\frac{\tau_b}{\rho H} \tag{7}$$

where $\hat{\mathbf{z}}$ is the vertical unit vector pointing upward, χ is a barotropic relative vorticity (1/s), ε_b is the energy dissipation rate associated with depth-induced wave breaking, $\mathbf{k}$ is a wavenumber vector, σ is an intrinsic wave frequency, ρ is the density of the fluid (= 1030 kg/m^3), $\mathbf{U}^{\mathbf{st}}$ is the depth-integrated Stokes drift velocity (*i.e.*, Stokes transport), and τ_b is the bottom drag stress. In the present study, we employ a linear drag model:

$$\tau_b=\rho\mu\mathbf{u} \tag{8}$$

with μ : a linear bottom drag coefficient (m/s), or a combined wave-current bed stress model by Soulsby (1995):

$$\tau_b=\tau_c\left[1+1.2\left(\frac{|\tau_w|}{|\tau_c|+|\tau_w|}\right)^{3.2}\right] \tag{9}$$
$$\tau_c=\rho\left[\frac{\kappa}{\ln(z_m/z_0)}\right]|\mathbf{u}|\mathbf{u};\quad \tau_w=\frac{1}{2}\rho f_w|\mathbf{u}_b|^2$$

where τ_c and τ_w are the bottom stresses due to currents and waves, κ is the von Kármán constant, z_m is a reference depth above the bed (= H/2), z_0 is the bed roughness length (= 1 cm), $\mathbf{u}_b$ is the RMS bottom wave orbital velocity,

$$\mathbf{u}_b=\frac{\sigma H_{rms}}{2\sinh kH}\frac{\mathbf{k}}{k} \tag{10}$$

where H_{rms} is the RMS wave height (= 2a), a is a wave amplitude, $k = |\mathbf{k}|$ is the magnitude of the wavenumber vector, and f_w is the wave friction factor:

$$f_w=1.39\left(\frac{\sigma z_0}{|\mathbf{u}_b|}\right)^{0.52} \tag{11}$$

$\mathbf{U}^{\mathrm{st}}$ and $\hat{\zeta}$ are estimated according to the weakly nonlinear wave theory with respect to the small wave slope ak as:

$$\mathbf{U}^{\mathrm{st}}=\frac{a^2\sigma\mathbf{k}}{2k\tanh kH}=\frac{1}{\rho}A\mathbf{k} \tag{12}$$

$$\hat{\zeta}=-\frac{a^2k}{2\sinh 2kH} \tag{13}$$

where $A = E/\sigma$ is the wave action density and $E=\rho g a^2/2$ is the depth-integrated wave energy.

Wave Model

For a narrow-banded spectrum-peak wave field, we exploit a set of the ray equations based on the WKB approximation (*e.g.*, Mei, 1994) for wave refractive transformation with a (band-integrated) wave action density conservation equation:

$$\frac{\partial A}{\partial t}+\nabla\left(A\mathbf{c}_{\mathrm{g}}\right)=-\frac{\varepsilon_b}{\sigma} \tag{14}$$

and a wave number conservation equation:

$$\frac{\partial\mathbf{k}}{\partial t}+\mathbf{c}_{\mathrm{g}}\cdot\nabla\mathbf{k}=-\left(\tilde{\mathbf{k}}\cdot\nabla\right)\tilde{\mathbf{u}}-\frac{k\sigma}{\sinh 2kH}\nabla H \tag{15}$$

along with the linear dispersion relation:

$$\sigma^2=gk\tanh kH\ ;\ \omega=\mathbf{u}\cdot\mathbf{k}+\sigma \tag{16}$$

The tilde convention in the wavenumber conservation identifies conjoined horizontal vectors in a dot product, and ω is a Doppler-shifted (CEW) wave frequency.

The associated Doppler-shifted group velocity is

$$\mathbf{c}_{\mathrm{g}}=\mathbf{u}+\frac{\sigma}{2k^2}\left(1+\frac{2kH}{\sinh 2kH}\right)\mathbf{k} \tag{17}$$

The breaker dissipation ε_b is determined by a quasi-empirical parameterization for Rayleigh distributed narrow banded waves described in Church & Thornton (1993):

$$\varepsilon_b = \rho g \frac{3\sqrt{\pi}}{16}\frac{B_b f_p}{H} H_{rms}^3 \left[1+\tanh\left\{8\left(\frac{H_{rms}}{\gamma_b H}-1\right)\right\}\right] \cdot\left[1-\left\{1+\left(\frac{H_{rms}}{\gamma_b H}\right)^2\right\}^{-\frac{5}{2}}\right] \quad (18)$$

where f_p is a peak wave frequency (= $\omega / 2\pi$), B_b and γ_b are empirical constants depending on beach topography and types of breaker. In the present study, B_b = 1.3 and γ_b = 0.38 are specified.

The phase-averaged hydrodynamic model and the wave model are tightly coupled to account for the two-way interaction between waves and currents. The conservative WEC appears in $\hat{\zeta}$, **J** and $\mathbf{U}^{st}$ and the non-conservative WEC are considered in **B** and **D**. The classical prescription based on radiation stress divergence for surf zone applications can be obtained by substituting the WKB wave dynamics into $\hat{\zeta}$ and **B** terms. In turn, CEW is considered in $\mathbf{c}_g$ and H in the ray equations.

Sediment Transport Model

The evolution of the topography is determined by the divergence of the horizontal sediment transport:

$$\beta\frac{\partial z_b}{\partial t}+\nabla\mathbf{q}=0 \quad (19)$$

where β is an acceleration factor (= 100) to enhance much slower temporal evolution of the morphological process than that of the current and wave fields, z_b is again the upward bed level perturbation measured from the initial resting depth h, and **q** is the depth-integrated, horizontal sediment flux based on the total (suspended and bed) load model of Soulsby and Van Rijn described in Soulsby (1997):

$$\mathbf{q}=\alpha\left\{\left(\mathbf{u}+\mathbf{u}^{st}\right)-\gamma|\mathbf{u}_b|\nabla z_b\right\} \quad (20)$$

where $\mathbf{u}^{st}$ is the depth-averaged Stokes drift velocity (= $\mathbf{U}^{st}/H$), γ is an empirical bed slope constant (= 10), and α is the stirring factor. Notice that the first half of the r.h.s, α (**u** + $\mathbf{u}^{st}$), is the sediment transport term proportional to Lagrangian velocity that is responsible for tracer advection (*e.g.*, Uchiyama *et al*., 2010). The second half is a downslope term that acts as diffusing z_b in the lateral direction to suppress instability associated with abrupt topography changes (Garnier *et al*., 2008).

The stirring factor α is expressed as:

$$\alpha=\begin{cases}\dfrac{1}{1-\lambda}A_s\left(u_s-u_c\right)^{2.4} & \text{for } u_s>u_c\\ 0 & \text{for } u_s\le u_c\end{cases} \quad (21)$$

where λ is the bed sediment porosity (= 0.4), u_c is the critical friction velocity beyond which the bed sediment transport is initiated,

$$u_c = 8.5\left(d_{50}\right)^{0.6}\log_{10}\left(\frac{4h_*}{d_{90}}\right) \quad (22)$$

with $h_* = h - z_b$, d_{50} is the median grain size of the bed sediments (= 0.25 mm), d_{90} = 0.50 mm is the 90-percentile grain size, u_s is the stirring velocity:

$$u_s=\left[|\mathbf{u}|^2+\frac{0.018}{\kappa}\ln\left(\frac{z_m}{z_0}\right)|\mathbf{u}_b|^2\right]^{\frac{1}{2}} \quad (23)$$

and A_s is an empirical factor of the joint contributions from bed load A_{sb} and suspended load A_{ss}, depending on sediment characteristic and water depth:

$$A_s = A_{sb}+A_{ss}=\frac{0.005H\left(d_{50}/H\right)^{1.2}}{\left[\left(1-s\right)gd_{50}\right]^{1.2}}+\frac{0.012d_{50}D_*^{-0.6}}{\left[\left(1-s\right)gd_{50}\right]^{1.2}} \quad (24)$$

where $s = \rho_s - \rho$ with the density of the sediments ρ_s = 2690 kg/m^3, and

$$D_* = \left[\frac{g\left(s-1\right)}{\nu^2}\right]^{\frac{1}{3}} d_{50} \quad (25)$$

is an effective grain size with ν the kinematic viscosity of the fluid (*viz*., 1.0 × 10^{-6} m^2/s).

Numerical Experiments

The governing equations are properly discretized and embedded in the barotropic version of ROMS (Regional Oceanic Modeling System, Shchepetkin & McWilliams, 2005; Uchiyama & McWilliams, 2008; Uchiyama *et al*., 2009). The wave and sediment models are solved synchronously with the hydrodynamic kernel of ROMS. The advective terms in the momentum equation is discretized with the first order upwind scheme and the time stepping of the morphological evolution depends on the second order Adams-Bashforth scheme. All the numerical experiments shown subsequently rely on

periodic boundary conditions in the alongshore direction. The onshore and offshore boundary conditions are specified with the flux-blocking condition and a Flather-type radiation condition with the cramped offshore waves.

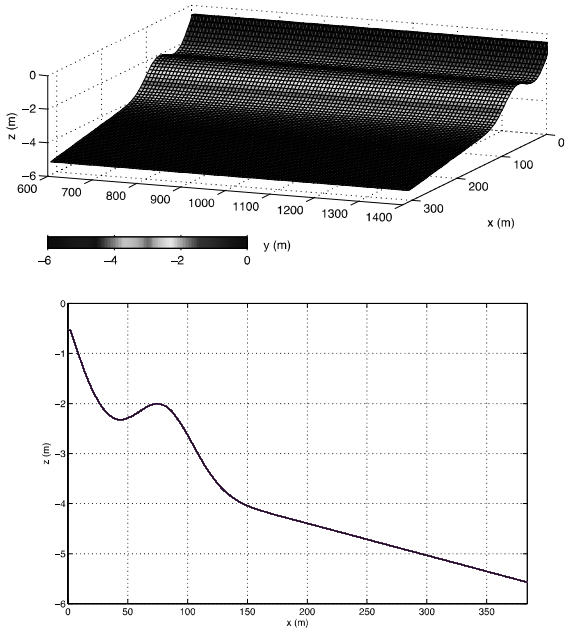

Fig. 1: Initial topography of an alongshore-uniform single barred beach mimicking a sandy beach in Duck, NC. The bar crest is located at $x = x_c = 80$ m. Top: a perspective view, bottom: the cross-shore bottom profile at $y = 924$ m.

In the present study, attention is paid to the cases with normal incident offshore waves leading to the strongest offshore-headed rip currents. The initial unperturbed topography mimicking a sandy beach in Duck, NC, USA, is introduced according to the mathematical expression by YS03:

$$h_1(x) = \left(a_1 - \frac{a_1}{\gamma_1}\right)\tanh\left(\frac{b_1 x}{a_1}\right) + \frac{b_1 x}{\gamma_1} - a_2 \exp\left[-5\left(\frac{x - x_c}{x_c}\right)^2\right] \quad (26)$$

where x_c determines the position of the bar crest (= 80 m), x is the cross-shore coordinate pointing offshore, a_1 = 2.97 m, a_2 = 1.5 m, $b_1 = \tan\beta_1$, $\gamma_1 = \tan\beta_1 / \tan\beta_2$, β_1 = 0.0075, and β_2 = 0.0064. The depth h_1 represents an alongshore uniform, straight coastline.

An alongshore heterogeneity is added as

$$h_2(x, y) = h_1(x)\left\{1 + \varepsilon\cos\left(\frac{2\pi y}{L_y}\right)\exp\left[-5\left(\frac{x - x_c}{x_c}\right)^2\right]\right\} \quad (27)$$

where ε is a small parameter to introduce an alongshore topographic periodicity in y (*viz.*, rip channels) with a prescribed alongshore topographic wavelength L_y

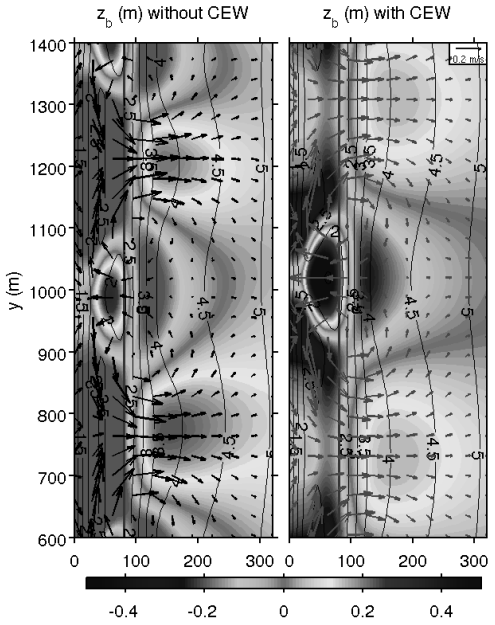

Fig. 2: Modeled topography on topographic model day 100 reaching a quasi-steady state. Left: without CEW, right: with CEW. Color: perturbation topography z_b where positive and negative values correspond to accretion and erosion, contours: mobile bottom topography $h^* = h - z_b$, and vectors: barotropic Eulerian velocity.

RESULTS AND DISCUSSION

Mobile Bed Experiment

The first result is from the mobile bed cases where the initial topography is set to be alongshore uniform as expressed by (26). The bed shear stress for current is acquired by the combined wave-current formula (9). The size of the domain is chosen to be 384 m (x) × 2048 m (y) with an anisotropic rectangular grid spacing of dx = 4 m and dy = 8 m. The barotropic time step is dt = 0.32 s and the time integration is made over 5 hydrodynamic model days, equivalent to 500 morphological model days as for the acceleration factor β = 100 in (19). The imposed offshore wave conditions are normal incidence with H_{rms} = 1.0 m and the peak wave period of 10 s. The initial unperturbed topography synthesized by (26) with x_c = 80 m is shown in **Fig. 1**. A grid-size (4 × 8 m) perturbation z_b is placed at (x, y) = (48, 1024) m with a height of 10 cm as a "seed" of instability on topographic model day 5 (*i.e.*, hydrodynamic model hour 1.2) when alongshore-uniform littoral currents and waves are fully developed. With the initial perturbation, sediment transport successfully occurs to yield a self-organization of the rip channels resulting in a quasi-steady alongshore

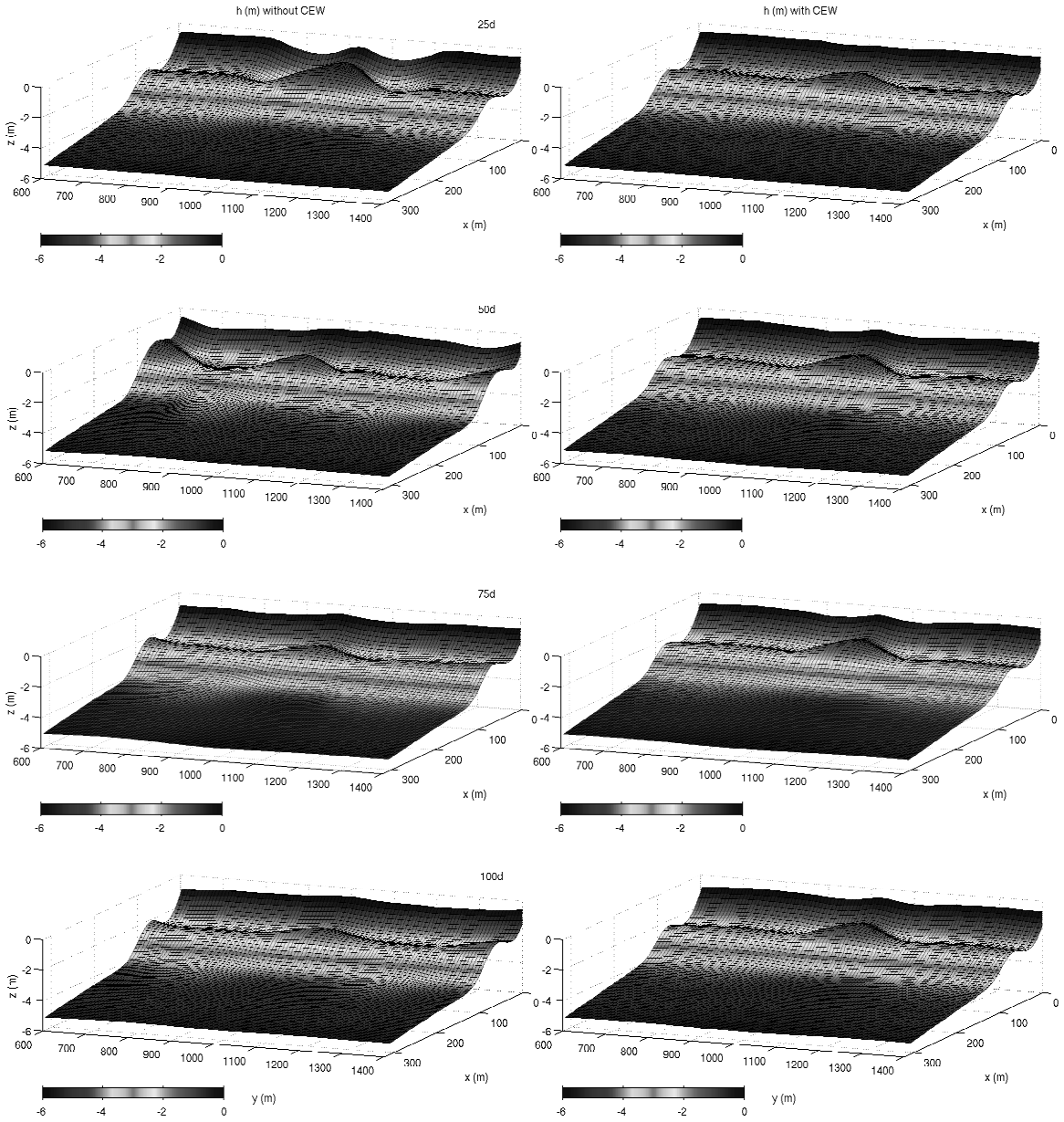

Fig. 3: Temporal evolution of the topography for the mobile bed cases on topographic model days 25, 50, 75 and 100 from top to bottom, respectively. Left panels: the case without CEW, right panels: with CEW.

periodicity on the topographic model day 100, either with or without CEW (**Fig. 2**). The temporal evolution of the rip channel system is demonstrated for the topographic model days 25, 50, 75 and 100 in **Fig. 3**.

Offshore-headed rip currents are formed in the deeper rip channels in the onshore side of the bar crest, while accretion takes place in the offshore of the crest beneath the rip heads creating a submerged crescent-shaped bar. Both the erosion and accretion along the rip channels is more evident for the case without CEW, consistent with larger rip currents (**Fig. 2**). In other words, CEW helps in widening and flattening the rip channels and submerged mounds formed just seaward of the bar crest. The rip currents return back towards the surf zone to enhance accretion that forms a mound between two rip channels (warm colors in **Fig. 2**). The height of this mound in the return flow region is greater for the case with CEW rather than for the case without CEW (**Fig. 2**). More importantly, the alongshore wavelength λ_y of the rip channel spacing becomes longer when CEW is taken into account. A variance-preserving spectral analysis (not shown) indicates λ_y = 400 m without CEW whereas λ_y = 500 m with CEW. These results exhibit that CEW decelerates rip currents

consistently with the finding of YS03, widens the rip channel spacing, and flattens the rip channel topography.

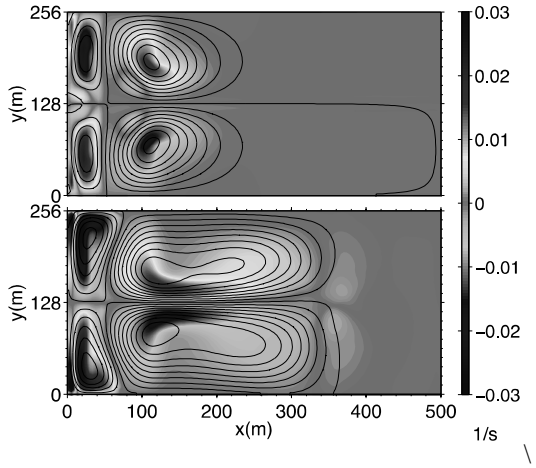

Fig. 4: Steady-state rip cell patterns (upper) with CEW and (lower) without CEW. Rip currents are attenuated in the offshore direction due to CEW, consistent with YS03 and Weir *et al*. (2011). Color: relative vertical vorticity of the Eulerian barotropic velocity; contours: iso-lines of stream function of the Lagrangian velocity. The rip channels are centered at y = 128 m.

Immobile Bed Experiment

Since we find that the sediment transport flux **q** is highly dominated by the transport term α (**u** + **u** st) and **u** >> **u** st (not shown), the associated morphology is considerably controlled by the wave-driven Eulerian velocity **u**. This suggests that modulations of the rip and longshore currents formed on the rip channel topography could be important for the noticeable modification of the beach morphology by CEW. Therefore a comparative experiment (with and without CEW) is conducted on the immobile barred beach topography with the prescribed rip channels represented by (27). This is equivalent to the canonical case in YS03, but with the more complete vortex force formalism as done by Weir *et al*. (2011). The alongshore wavelength L_y = 256 m (*viz*., the rip channel spacing), ε = 0.1, dx = dy =4 m, and the linear bottom drag (8) with μ = 0.002 m/s are specified for this experiment.

Figure 4 clearly illustrates reduction of the offshore extent of rip currents due to CEW, consistent with the results of YS03 and Weir *et al*. (2011). According to the momentum budget analysis (not shown), this is certainly caused by CEW. The enhanced wave height near the bar crest in the rip channels and wave ray bending (refraction) by currents lead to an increase of the breaker wave dissipation ε_b (*n.b.*, the acceleration for currents) and changes in the pressure gradient force through the modified wave set-up/down distribution. All these modification by CEW play roles in attenuating the offshore extent of the rip currents, resulting in reduction of the offshore sediment transport and widening the rip channel spacing.

SUMMARY

A coupled, barotropic wave-current-sediment model is developed to successfully reproduce the alongshore periodic rip channel topography with normal incident offshore waves. We exhibit the rip current reduction by CEW on an immobile single barred beach with equally spaced rip channels. Among the other CEW such as the Doppler shift and wave set-down/up, wave refraction on currents is found to be most important in modifying the wavenumber field and breaker dissipation, leading to a systematic modulation in the diagnostic momentum balance. An alongshore-uniform barred topography evolves into a rhythmic rip channel system through intrinsic instability triggered by a small disturbance. We demonstrate that CEW is responsible for widening the rip channel spacing, shoaling the rip channel in the surfzone, and shrinking submerged crescent mounds in the offshore beneath rip heads.

ACKNOWLEDGEMENTS

This work is financially supported by the Grant-in-Aid for Scientific Research (#24560622 and #25110508).

REFERENCES

Church, J. C., and Thornton, E.B. (1993). Effects of breaking wave induced turbulence within a longshore current model, *Coastal Eng.*, 20: 1-28.

Garnier, R., Calvete, D., Falqués, A. and Dodd, N. (2008). Modelling the formation and the long-term behaviour of rip channel systems from the deformation of a longshore bar. *J. Geophys. Res.*, 113, C07053, doi:10.1029/2007JC004632.

Haas, K. A., Svendsen, I.A. and Haller, M.C. (1999). Numerical modeling of nearshore circulations on a barred beach with rip channels, paper presented at *26th Conference on Coastal Engineering*, Am. Soc. of Civ. Eng., Copenhagen, Denmark.

Mei, C.C. (1994). *The applied dynamics of ocean surface waves*, World Scientific, Singapore, 740 pp.

McWilliams, J.C., Restrepo, J.M. and Lane, E.M. (2004). An asymptotic theory for the interaction of waves and currents in coastal waters. *J. Fluid Mech*. 511: 135– 178.

Özkan-Haller, H. T., and Y. Li (2003). Effects of wave-current interaction on shear instabilities of longshore currents, *J. Geophys. Res.*, 108 (C5), 3139, doi:10. 1029/2001JC001287.

Shchepetkin, A.F. and McWilliams, J.C. (2005). The Regional Oceanic Modeling System: a split-explicit,

free-surface,topography-following-coordinate oceanic model, Ocean Modell. 9, 347–404.

Soulsby, R. L. (1995). Bed shear-stresses due to combined waves and currents, in *Advances in Coastal Morphodynamics*, Eds. M. Stive *et al*., Delft Hydraul., Delft, Netherlands: 4-20–4-23.

Soulsby, R. L. (1997). *Dynamics of Marine Sands*, A Manual for Practical Applications , 249 pp., Thomas Telford, London.

Uchiyama, Y. and McWilliams, J.C. (2008). Infragravity Waves in the Deep Ocean: Generation, Propagation, and Seismic Hum Excitation, *J. Geophys. Res.*, 113, C07029, doi:10.1029/2007JC004562.

Uchiyama, Y., McWilliams, J.C. and Restrepo, J.M. (2009). Wave-current interaction in nearshore shear instability analyzed with a vortex-force formalism, *J. Geophys. Res.*, Vol. 114, C06021, doi:10.1029/2008 JC005135.

Uchiyama, Y., McWilliams, J.C. and Shchepetkin, A.F. (2010). Wave-current interaction in an oceanic circulation model with a vortex force formalism: Application to the surf zone, *Ocean Modell.*, Vol. 34:16-35.

Weir, B., Uchiyama, Y., Lane, E.M., Restrepo, J.M. and McWilliams, J.C. (2011). A vortex-force analysis of the interaction of rip currents and gravity waves, *J. Geophys. Res.*, Vol. 116, C05001, doi:10.1029/2010 JC006232

Yu, J., and D. N. Slinn (2003). Effects of wave-current interaction on rip currents, *J. Geophys. Res.*, 108 (C3), 3088, doi:10.1029/2001JC001105.